Electronic Processes in Oxide Cathodes

T. N. Chin

RCA Electronic Components, Princeton, N.J. 08540

R. W. Cohen and M. D. Coutts

RCA Laboratories, Princeton, N.J. 08540

Abstract—The rising interest in the use of high-current-density emitters in electron-beam devices prompts further consideration of the electronic processes in an oxide cathode. This paper begins with a brief review of the relevant characteristics of the alkaline-earth oxides used for thermionic emission. The proposed, idealized model in which ion adsorption occurs on the crystalline surfaces accounts for the emission characteristics and the conductivity of the oxide coating. It is possible to correlate the measured values from oxide crystals with those of oxide coatings by using a simplified analysis. Also, some of the underlying limitations in the cathode operations are revealed and discussed in connection with this model.

1. Introduction

There has been extensive work on oxide cathodes concerning various aspects of the operating properties. Most of the early efforts were directed toward those cathodes coated with the crystalline oxide powders. Later investigations on single crystals of barium oxide provided much of the understanding of the semiconducting properties of this compound. A summary of the experimental progress and the theories advanced to explain the operating mechanisms may be obtained from Refs. (1)–(8).

Most of the recent studies pursued the subject from the point of

view of defect chemistry.[9] While experiments are performed to examine the chemical properties of these oxides, the correlation with the operation of a real oxide cathode is yet to be completely determined. The lack of a widely accepted physical model indicates the complexities involved in the cathode operation.

For many years oxide-coated cathodes have been almost universally used in the cathode-ray[10] and other electron-beam[11] vacuum tubes. At present, the oxide cathode is still of considerable practical importance as an electron emitter. In this paper, a simple model is proposed to explain the electronic processes in an oxide cathode. Through a simplified analysis, we estimate and correlate the observed characteristics with the experimentally obtained parameters.

2. Physical Background

2.1 Oxide Coating

Although it is not necessary here to describe the detailed preparation of an oxide-coated cathode, some important characteristics of the oxides are outlined in order to deduce an idealized model. At present the oxide coatings are commonly prepared from the triple carbonates $(BaSrCa)CO_3$. Generally, they consist of about equal amounts of the barium and the strontium carbonates with a small quantity of calcium carbonate. Two types of carbonate particles precipitated from two different solutions are shown in Figs. 1 and 2. The coating density on the cathode surface ranges from 4 to 8 mg/cm^2. For a coating of 2–3 mils thick, there may be 15 to 30 layers of carbonate particles.

The porosity of such an oxide coating usually varies between 20 and 50%. The texture of a typical carbonate coating is given in Fig. 3. Since the carbonates are highly insulating, some charging problems are noticeable in the scanning electron micrograph (SEM). By using the conventional procedure, the carbonate coating is then converted and activated. At the end of activation, the electron current density reaches about 0.5 ampere/cm^2 at 1100°K. When the cathode is at high temperatures, the contrast of SEM pictures is inadequate to show the oxide crystallites. The photograph in Fig. 4 was taken a few seconds after the cathode heating was turned off in order to reveal the activated oxide crystallites.

2.2 Conductivity Data

In addition to the electron emission measurement, the conductivity of the oxide coating has been repeatedly measured by different ap-

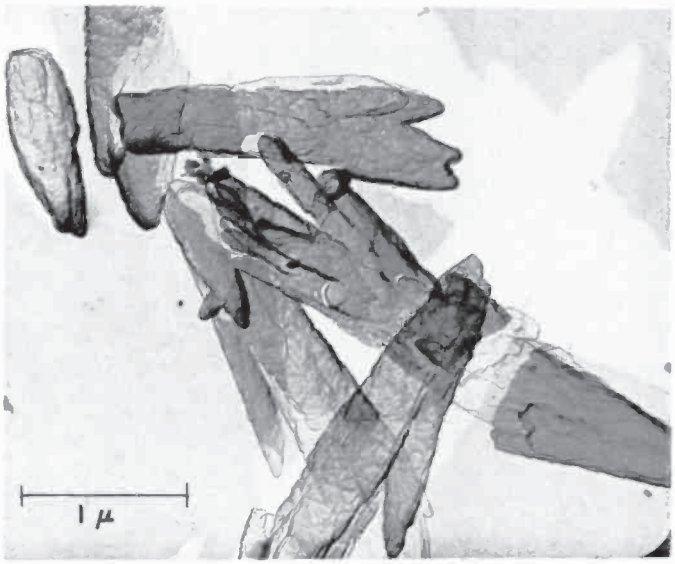

Fig. 1—Sodium-precipitated triple-carbonate crystallites photographed using the carbon-replica technique.

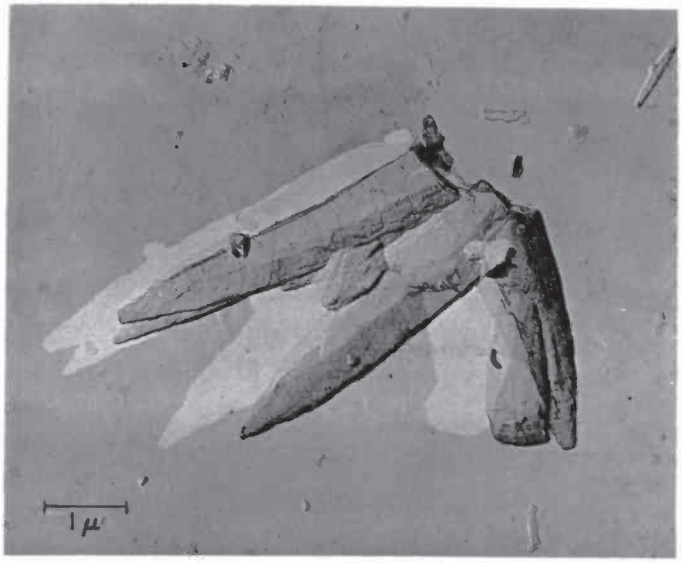

Fig. 2—Ammonium-precipitated triple-carbonate crystallites photographed using the carbon-replica technique.

Fig. 3—SEM photograph of a triple-carbonate coating on a planar cathode before activation; original magnification ×10000 (photo reduced by approximately 15% in printing).

proaches as reported in the literature. Selected values from these measurements appear in Table 1, which gives a list of mean values for the conductivity of single crystals,[12–15] BaO crystallites,[16,17] and (Ba,Sr)O coatings.[18] As with many other polycrystalline materials, the measurements to determine the conductivity are difficult to per-

Table 1—Values of Electrical Conductivity at 1100°K of Alkaline-Earth Crystals and Coatings

	Conductivity $(\text{ohm-cm})^{-1}$
BaO Single Crystal[12,13]	$1–2 \times 10^{-4}$
SrO Single Crystal[14]	10^{-7}
CaO Single Crystal[15]	10^{-8}
Unactivated BaO Coating[16,17]	$10^{-5}–10^{-4}$
Activated BaO Coating[5,16]	$1–5 \times 10^{-2}$
Unactivated (Ba,Sr)O Coating[18]	$3 \times 10^{-6}–10^{-4}$
Activated (Ba,Sr)O Coating[18]	$2 \times 10^{-3}–10^{-2}$

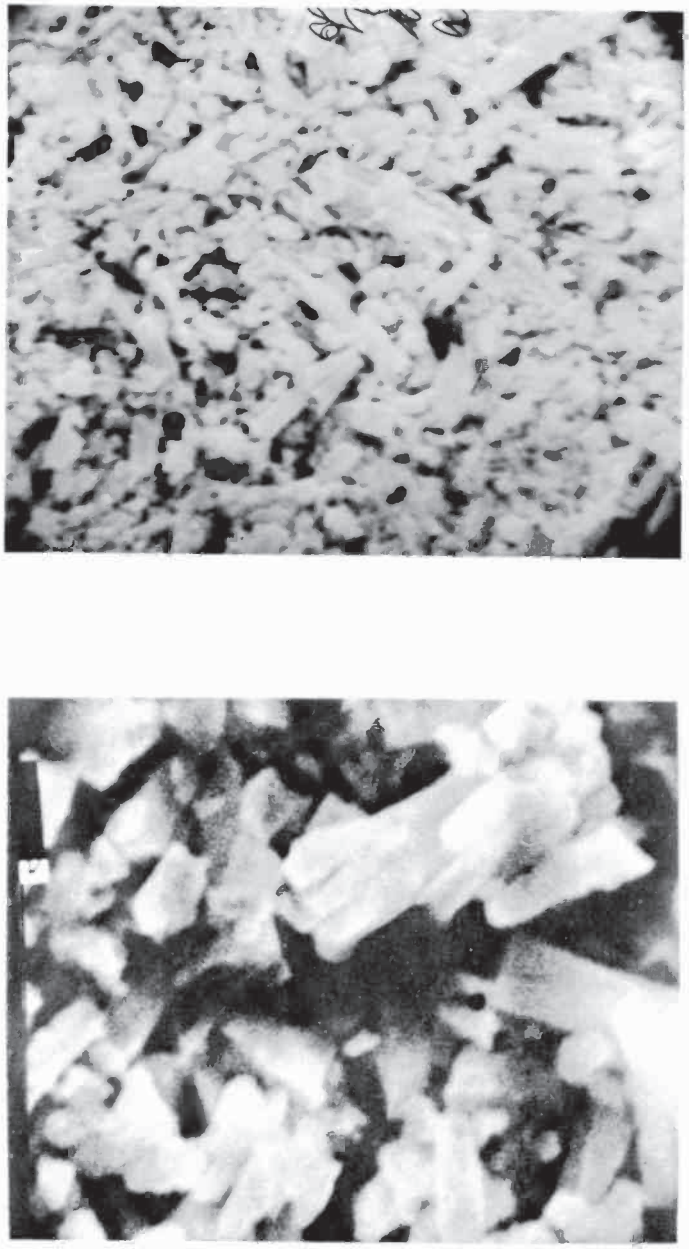

Fig. 4—SEM photographs of triple-oxide crystallites on a planar cathode after activation; original magnifications: (a) ×5000, (b) ×20000 (photo reduced by approximately 15% in printing).

form, and some deviations may occur because of variations in the coating, such as the chemical inhomogeneity and the porosity or contaminations. However, we note for future reference that the conductivity of BaO crystals is about two orders of magnitude lower than that of activated BaO layers.

2.3 Emission vs. Conductivity

In the case of oxide coatings, several investigators[18] have concluded that the electron emission and the electrical conductivity of an oxide-coated cathode are linearly related at each state of activation. For this discussion, it is not necessary to include the pore conduction process, which becomes significant at very high temperatures. Considerable work on photoemission has been reported, but far fewer investigations have been carried out on the thermionic emission properties of BaO crystals. A similar relationship between the thermionic electron emission and the electrical conductivity was sought in the experimental study of BaO crystals. However, little correlation[19] could be established between the electron emission and the electrical conductivity for BaO crystals. This may be additional experimental evidence that the electrical conductivity measured from the oxide coating cannot be interpreted as a bulk property of these oxides.

2.4 Ion Adsorption Effects

In the early studies on the emission characteristics from monatomic layers, such as Cs, Th, and Ba on tungsten emitters, it was deduced[20] that any damage to the surface film, either by evaporation or by oxidation, destroys the emission. Because of the complexity involved in an actual oxide cathode, it is only recently[8] that the adsorption of barium has been identified as an essential factor in thermionic cathodes. Since the evaporation of BaO takes place at a much faster rate than that of SrO and CaO, the adsorption of barium ions on the strontium–calcium oxide is believed to be the activation process in a triple-oxide cathode.

From the texture and activation of the triple oxides, it is evident that barium adsorption can also take place on the interfaces between oxide crystallites. The porosity in the oxide coating allows the formation of such adsorbed interfaces in the same manner as that of the emitting surface. Consequently, electron accumulation will occur at these ion-adsorbed interfaces as well as in the emitting area of the oxide crystallites. As a result the barium adsorption serves not only to increase the electron emission at the cathode surface but also to

enhance the electron conductivity between the oxide crystallites. With the above assumption it is conceivable that the rate of barium-ion adsorption at the interfaces is equal to that at the emitting surfaces. This would explain the linear relation of electron emission and conduction found in these experiments.[18] Since the electron conductivity of BaO crystals cannot be increased through this adsorption process, the relationship of the thermionic emission with the electron conductivity is not expected to be linear. Hence, it is not surprising that the conductivity of the activated-oxide layer is two orders of magnitude higher than that of BaO crystals at high temperatures.

3. Simplified Analysis

3.1 An Idealized Model

With the adsorbed ions throughout the interfaces, the conducting paths along the crystallites are illustrated schematically in Fig. 5. The

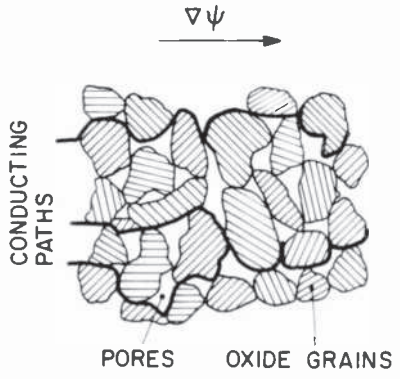

Fig. 5—The structure of oxide grains in a real cathode.

observed conductivity is the sum of these paths along the interfaces of the oxide crystallites. In order to facilitate the estimation of the conductivity of the coating, the oxide crystallites are depicted in Fig. 6 as simple cubes with an edge width D. For simplicity, these identical cubes are stacked in a regular array with some separation between them in each layer. The separations, as indicated in this model, simulate the porosity of a real oxide coating on the cathode. Also, separations are shown only between grains in each layer and not between layers. This is really a simplification rather than an indication of any anisotropy in the formation of the coating.

From this idealized model, it is obvious that the lengths of the conducting paths are not greatly increased from the apparent thickness of the oxide coating. The conductance G of the coating is a sum of the contributions of all the paths i,

$$G = \sum_i \frac{\sigma a_i}{l_i} \cong \frac{\sigma}{l} \sum_i a_i,$$

where the conductivity σ along the path is considered the same for all

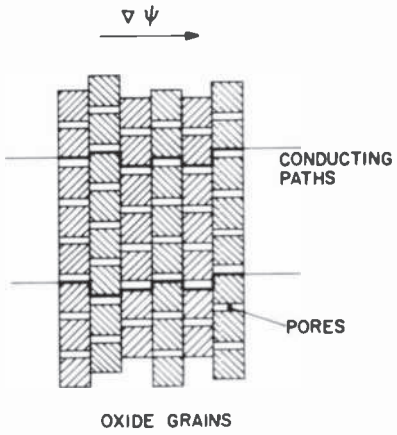

Fig. 6—A simplified model for the oxide grains in the cathode coating.

paths, l is the thickness of the coating, and a_i is the cross-sectional area of the conducting part of the grains. Although this estimate is valid only for cubes, the same reasoning can be employed to approximate the conductivity for grains of other shapes.

In accordance with the simplified model, the path of conductance G is parallel to the electric field, as shown in Fig. 6. A schematic diagram, Fig. 7, of the cross section taken through the oxide grains in a layer illustrates the conductive surface layer on the cubic grains. If the surface layer[21] of cubes is the major conductive part, the cross-sectional area of the conducting path is actually $4L(D-L)$ instead of D^2, the geometric cross section of the cube. Here, L is the approximate depth of the surface layer where the conductivity is greatly enhanced due to the ion adsorption. It will be shown later that for an unactivated grain the effective length L may reach $D/2$, so that electron conduction can be nearly uniform throughout the grain. The

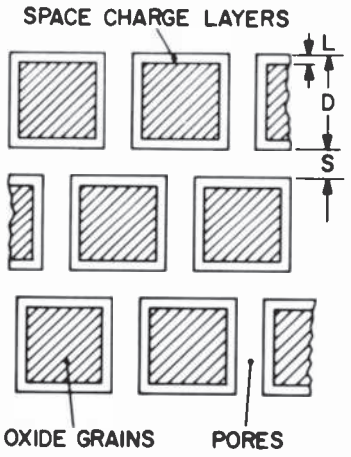

Fig. 7—A cross-sectional view of the oxide grains in a well-activated cathode.

thickness L of the surface layer will decrease as the barium adsorption progresses. In a well-activated coating, the value of L is expected to be only a small fraction of the grain size D.

3.2 Calculation of Space-Charge Accumulation

When the cathode is well activated, the free carriers accumulated at the surface will reach a quasi-equilibrium[22] condition. In Fig. 8, the

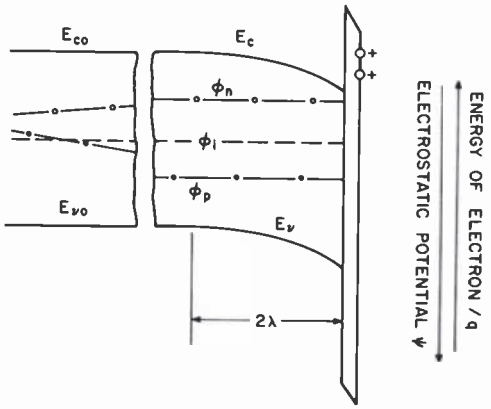

Fig. 8—The energy-level diagram at the surface of a well-activated oxide grain.

energy band edges E_c and E_v near the surface illustrate the effect of space charge accumulation, i.e.,

$$E_c(x) = E_{co} - q\psi(x),$$

and

$$E_v(x) = E_{vo} - q\psi(x),$$

where E_{co} and E_{vo} are the conduction and valence band edges in the bulk, q is the electronic charge, and ψ is the electrostatic potential. In this one-dimensional case, it is convenient to have the coordinate x directed toward the outside surface and to arbitrarily choose

$$\psi = 0,$$

and

$$\frac{d\psi}{dx} = 0$$

at the left boundary, not shown in Fig. 8, where $x = 0$.

In the nondegenerate case, the electron density at the surface can be described by

$$\begin{aligned} n &= n_i \exp\left(\frac{\phi_n - \phi_i}{kT}\right)\exp\left(\frac{q\psi}{kT}\right) \\ &= n_e \exp\left(\frac{q\psi}{kT}\right), \end{aligned} \qquad [1]$$

where n_e is the effective electron density in the bulk after the activation. As shown in Fig. 8, ϕ_i is the intrinsic Fermi level, and ϕ_n and ϕ_p are the quasi-Fermi levels for electrons and holes and in the well-activated condition. For a semiconductor with a dielectric constant κ, Poisson's equation is

$$\frac{d^2\psi}{dx^2} = \frac{4\pi q}{\kappa} n_e \exp\left(\frac{q\psi}{kT}\right). \qquad [2]$$

After substituting the dimensionless quantity

$$V = \frac{q\psi}{kT},$$

Eq. [2] can be simplified in the form

$$\frac{d^2V}{dx^2} = \lambda^{-2}\exp(V). \qquad [3]$$

where

$$\lambda = \sqrt{\frac{\kappa kT}{4\pi q^2 n_e}}. \qquad [4]$$

Here the characteristic quantity λ is the usual Debye length. After the first integration, Eq. [3] may be reduced to

$$\left(\frac{dV}{dx}\right)^2 = 2\lambda^{-2}\exp(V) + C_1. \qquad [5]$$

Evaluating C_1 with the boundary condition,

$$\left(\frac{dV}{dx}\right) = 0 \quad \text{at } V = 0,$$

one obtains

$$\frac{dV}{dx} = \frac{\sqrt{2}}{\lambda}(e^V - 1)^{1/2}. \qquad [6]$$

After the second integration, Eq. [6] becomes

$$2\sin^{-1}(e^{-V/2}) = \sqrt{2}\frac{x}{\lambda} + C_2. \qquad [7]$$

After using the boundary condition $V = 0$ at $x = 0$ to determine C_2, Eq. [7] can be written as

$$V = -2\ln\left[\cos\left(\frac{x}{\sqrt{2}\lambda}\right)\right] \qquad [8]$$

for

$$0 < x < \frac{\pi\lambda}{\sqrt{2}}$$

With this potential distribution at the surface, the potential gradient in the space-charge region is given by

$$\frac{dV}{dx} = \frac{\sqrt{2}}{\lambda}\tan\left(\frac{x}{\sqrt{2}\lambda}\right). \qquad [9]$$

and the space-charge density ρ in coulombs per cm^3 may be obtained from

$$\rho = \frac{qn_e}{\cos^2\left(\frac{x}{\sqrt{2}\lambda}\right)}. \qquad [10]$$

The general characteristics of the functions in Eqs. [8], [9], and [10] are shown graphically in Fig. 9. After integrating the charge density ρ

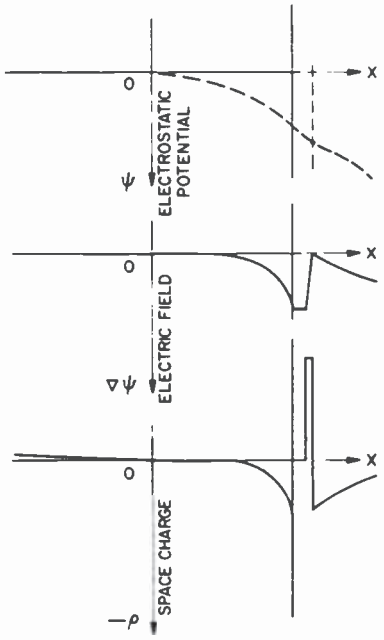

Fig. 9—The electrostatic potential, the electric field, and the space-charge distributions at the oxide surface.

up to the surface with the coordinate X, the total space charge Q in coulombs/cm^2 can be expressed as

$$Q = \sqrt{2}\lambda q n_e \tan\left(\frac{X}{\sqrt{2}\lambda}\right). \qquad [11]$$

Since the free charge in the grain before the activation is small, Eq. [11] is an approximate measure of the total adsorbed ions at the sur-

face. The maximum concentration of adsorbed barium ions would depend upon the chemical conditions of the oxide surface. Physically, it is the adsorbed positive charges that create the charge accumulation and the band bending in the surface layer.

3.3 Numerical Evaluations

Based upon the foregoing treatment, the characteristics of these oxides can be examined by using the experimentally obtained values from the literature.[23,24] From the measurements on BaO single crystals, the electron mobility μ in these oxides will be assumed[12] to be 5 cm^2/volt-sec.

(a) Unactivated Oxides

At the operating temperature of 1100°K, the electron density evaluated from the measured conductivity of unactivated oxides is not greatly increased from the intrinsic value of the material at that temperature as indicated in Table 2. Since there is no charge accumula-

Table 2—Physical Constants and Parameters for Alkaline-Earth Oxides

	BaO	SrO	CaO
Bandgap E_g (eV)	$4.4-0.001\,T$	$5.9-0.001\,T$	$7.6-0.001\,T$
Dielectric Constant (κ)	34	13.1	11.1
n_i at 1100°K (cm^{-3})	4.7×10^{12}	1.69×10^{9}	2.1×10^{5}
Unactivated σ_o $(ohm\text{-}cm)^{-1}$	10^{-5}	3×10^{-6}	
n_o (cm^{-3})	1.25×10^{13}	3.75×10^{12}	
$E_c - \phi_o$ (eV)	1.56	1.65	
$\phi_o - \phi_i$ (eV)	0.09	0.75	
λ (μm)	3.78	4.28	

tion at the crystallite surface, the energy-band diagram is that shown in Fig. 10. If the bandgap energies[8,25,26] given in Table 2 are used in the calculation, the quasi-Fermi level will be more than 1.5 eV below the conduction band. This deduction agrees with the views commonly expressed that these oxides are slightly n-type[13] with only small concentration of ionized donors at the operating temperature.

Before the oxides are activated, the electron conduction is assumed to be nearly uniform throughout the grain. The apparent electron density n_o will be equal to the effective density n_e in the grain. The

calculated densities at 1100°K are listed in Table 2. The case of (BaSr)O crystallites may be considered as an intermediate case between that of BaO and SrO as shown here. If the dielectric constants given in Table 2 are used, the corresponding Debye lengths λ can also be computed and are listed for the cases in consideration.

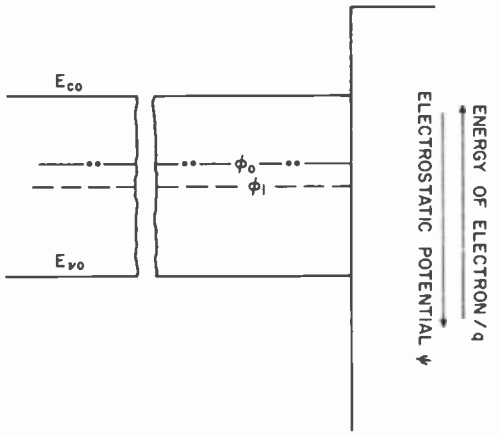

Fig. 10—The energy-band diagram at the surface of an unactivated oxide grain.

(b) Activated Oxides

For well-activated crystallites, the conductivity (Table 1) is about 2×10^{-3} (ohm-cm)$^{-1}$ at a temperature of 1100°K. Consequently, the apparent electron density n_a in the well-activated coating becomes

$$n_a = \frac{\sigma}{\mu q} = 2.5(10)^{15}\text{cm}^{-3}.$$

As a result of the space-charge accumulation on the oxide crystallites, the electron density n_b at the beginning of the surface layer where $x = 0$ may be estimated from

$$n_b = \frac{n_a D^2}{4L(D - L)} \qquad [12]$$

according to this idealized model.

For an average size $D = 5\ \mu$m and $n_a = 2.5 \times 10^{15}$ cm^{-3}, the values of n_b for five L's are listed in Table 3. For each of these values of n_b,

Table 3—Estimated Layer Thickness and Debye Length

L (μm)	n_b (cm^{-3})	λ (μm)
1	3.9×10^{15}	0.13
0.4	8.5×10^{15}	0.09
0.2	1.6×10^{16}	0.066
0.1	3.2×10^{16}	0.046
0.05	6.3×10^{16}	0.033

the corresponding Debye length λ can be calculated from Eq. [4] and is given in the last column. In view of the potential distribution, Eq. [8], it is well to approximate L to be twice the Debye length. For this activation condition, the correct thickness L is then between 1000 and 500 Å.

To examine the space-charge accumulation layer, Eqs. [8]–[11] are now evaluated in terms of the dimensionless quantity (X/λ). Values for four different surface layers are listed in Table 4 to indicate the increasing extent of the ion adsorption effects. If the adsorbed ions are singly charged, the last entry in the table represents the complete coverage by a monolayer of ions at the surface of the grain. According to the electrostatic fields, the voltage breakdown at the surface would occur before reaching the condition of the last entry. This may have been one of the sources that caused the voltage breakdowns[27] in the operation of oxide-coated cathodes.

While the electron density n_b is relatively moderate, Table 4 indicates that very high electric fields at the surface can occur as a result of positive ion adsorption. In taking λ = 500 Å, the major portion of

Table 4—Electronic Parameters for Space-Charge Surface Layers

$\frac{X}{\lambda}$	V	ψ (volts)	$\left(\frac{d\psi}{dx}\right)\left(\frac{\text{volt}}{\text{cm}}\right)$	$\frac{\rho(X)}{qn_e}$	$\frac{Q}{q}$ cm^{-2}
2.00	3.71	0.35	1.6×10^{5}	41	3×10^{12}
2.20	8.32	0.79	1.7×10^{6}	4.3×10^{3}	3.1×10^{13}
2.21	9.62	0.91	3.1×10^{6}	1.5×10^{4}	5.8×10^{13}
2.22	13.80	1.31	2.5×10^{7}	10^{6}	4.7×10^{14}

the sharp bending of energy band takes place only in the last 100 Å. If the value $n_b = 10^{16}$ cm^{-3} is taken at the left boundary of the accumulation layer, the possible electron density at the surface may reach 10^{20} cm^{-3}. Although impurities may contribute to the conductivity of unactivated crystallites, it is unlikely that they play a significant role if the electron density at the surface is so high.

4. Conclusion

Since Ba is the least electronegative (0.9) element of the alkaline-earth metals, the exposed Ba on the oxide crystallites will probably become a positive ion on the surface. In n-type semiconducting material, the adsorption of the positive ion will cause the energy levels to bend downward (Fig. 8) toward the surface. A similar condition was pointed out that the adsorption of O_2 in the Cu_2O lattice[28] attracts mobile holes toward the surface and thus enhances[29] the conductivity. It is also likely that Zn in hot-pressed ZnSe[30] diodes may play the same role in facilitating electronic injection and in assisting electrical conduction through the samples.

In the simple energy diagram, Fig. 8, the energy levels of the adsorbed ion are schematically indicated to be well above ϕ_n, the quasi-Fermi level. This is intended to show that the electron transfer between the space-charge layer and the adsorbed ions at the surface reaches detailed balance in the steady-state condition. As a consequence, a constant number of adsorbed ions remain at the surface, thus maintaining the space-charge accumulation. It may be expected that the ion adsorption effects should be similar in the cases of Ba on SrO, Ba on CaO,[31] and Ba on (BaSrCa)O. The work function of the oxides increases in the order from BaO, SrO, to CaO. Based upon the experimental findings, SrO with Ba ion adsorption seems to produce the highest emission density from the well-activated crystallites.

In the photoemission experiment,[32] the threshold energy of BaO was determined to be approximately 5.1 eV. For BaO, the bandgap energy at 300°K is 4.1 eV and therefore the electron affinity is about 1 eV. From this simplified analysis, this quasi-Fermi level is about 0.9 eV below the conduction band, and the band bending due to positive ion adsorption may be as high as 0.9 eV. If the experimental value[33] of the thermionic work function of this surface is 2.2 eV, then the effective electron affinity is about 1.3 eV, a reasonable value for SrO.

In the case of metallic emitters where the free electron density is of the order of 5×10^{22} cm^{-3}, the electron emission is most sensitive to the effective work function at the operating temperature. The adsorption phenomena[34] on metal (e.g., Cs on W, Ba on W) can be ex-

perimentally demonstrated with a true maximum emission region (S-shaped curve) as the operating temperature is varied. For Ba adsorption on BaO and SrO, only an abrupt change of the emission characteristics was obtained in the experiment as shown in Fig. 3 of Ref. [33]. This may be explained by the interdependence of the space-charge density and the adsorbed ions at the surface. As the temperature is raised to the extent that some desorption of Ba takes place, there is still a continuous increase in the free-electron density so that no maximum emission appears in the measured characteristics.

Since mobile carriers are attracted toward the surface of the oxide crystallite, the electrical conductivity is principally determined by that of the space-charge layer. By using this adsorption hypothesis, shallow donors are no longer required to explain the electrical conductivity of the oxide coating. As illustrated in the numerical example, the electronic properties of the activated oxide layer—one or two Debye lengths[35] at the surface—become most important in the operation. In future developments on oxide emitters, this area deserves more effort in the pursuit of improvements.

If oxygen vacancies exist at the surface, they would behave as donors and become the source of electrons for the space-charge layer. But if barium vacancies occur at the surface, they would act as acceptors and hence produce a compensation[36] effect. In essence, the acceptors would reduce the density of the free electrons at the surface space-charge layer. Since these barium vacancies will drift towards the surface due to the electrostatic field, this type of lattice defect might be an important deterioration factor to the operation of an oxide-coated cathode.

Since the electron density at the surface can be very high, a small density of surface states does not alter the qualitative description presented here. At present, the surface properties of these alkaline-earth crystals are not clear; it is difficult to explore the conditions of possible stable sites for the adsorbed ions. Further knowledge of the surface[37] layers will be valuable in clarifying the details of the operating mechanisms and in deducing the atomic structure—SrO, O, and Ba—at the surface of oxide crystallites.

Acknowledgment

The authors are indebted to E. P. Bertin for the use of unpublished pictures in Figs. 1 and 2, and to R. Williams for a critical reading and comments concerning the manuscript.

References:

[1] S. Dushman, "Thermionic Emission," *Rev. Mod. Phys.*, **2**, p. 381, (1930).

[2] A. L. Reimann, *Thermionic Emission*, p. 188, Chapman and Hall, Ltd., London, (1934).

[3] J. P. Blewett, "The Properties of Oxide-Coated Cathodes," *J. Appl. Phys.*, **10**, p. 668 and p. 831, (1939).

[4] A. S. Eisenstein, "Oxide Coated Cathodes," in *Advances in Electronics*, Academic Press, Inc., New York, (1948).

[5] G. Hermann and S. Wagener, *The Oxide Cathode*, Vols. I. and II, Chapman and Hall, Ltd., London, (1951).

[6] W. B. Nottingham, "Thermionic Emission," p. 97 in *Encyclopedia of Physics*, Springer-Verlag, New York, (1956).

[7] L. S. Nergaard, "Electron and Ion Motion in Oxide Cathodes," p. 154 in *Halbleiterprobleme*, Vieweg, Braunschweig (1956).

[8] P. Zalm, "Thermionic Cathodes," p. 211 in *Advances in Electronics and Electron Physics*, Academic Press, Inc., New York, (1968).

[9] F. Kroger, *Chemistry of Imperfect Crystals*, p. 564, John Wiley (1964).

[10] I. G. Maloff and D. W. Epstein, *Electron Optics in Television*, McGraw-Hill Book Co., New York, (1938); V. K. Zworykin, G. A. Morton, E. G. Ramberg, J. Hillier, and A. W. Vance, *Electron Optics and the Electron Microscope*, John Wiley and Sons, New York, (1954).

[11] J. R. Pierce, *Theory and Design of Electron Beams*, p. 145, Van Nostrand (1949); G. R. Brewer, "High-Intensity Electron Guns," p. 23 in *Focusing of Charged Particles*, Academic Press, Inc., New York, (1967).

[12] E. M. Pell, "The Hall Effect in Single Crystals of Barium Oxide," *Phys. Rev.*, **87**, p. 457, (1952).

[13] R. T. Dolloff, "Electrical Conductivity of Barium Oxide Single Crystals as a Function of Temperature and Excess Barium Density," *J. Appl. Phys.*, **27**, p. 1418, (1956).

[14] W. D. Copeland and R. A. Swalin, "Studies on the Defect Structure of Strontium Oxide," *J. Phys. Chem. Solids*, **29**, p. 313, (1968).

[15] N. A. Surplice, "The Electrical Conductivity of Calcium and Strontium Oxides," *Brit. J. Appl. Phys.*, **17**, p. 175, (1966).

[16] W. Meyer and A. Schmidt, "Über die Elektrizitatsleitung von Bariumoxyd in Zusammenhang mit der Elektronenmission," *Z. Tech. Phys.*, **13**, p. 137, (1932).

[17] H. J. Spanner, "Über die Thermische Emission Elektrisch Geladener Teilchen," *Ann. Phys.*, **75**, p. 609, (1924).

[18] N. B. Hannay, D. Macnair, and A. H. White, "Semiconducting Properties in Oxide Cathodes," *J. Appl. Phys.*, **20**, p. 669, (1949); R. Loosjes and H. J. Vink, "The Conduction Mechanism in Oxide-Coated Cathodes," Philips Res. Rep. 4, p. 449, (1949).

[19] E. O. Kane, Thesis, Cornell Univ., Ithaca, N.Y. (1953).

[20] L. R. Koller, "Electron Emission from Oxide Coated Filaments," *Phys. Rev.*, **25**, p. 671, (1925).

[21] A. R. Hutson, "Semiconducting Properties of Some Oxides and Sulfides," p. 543 in *Semiconductors*, Reinhold Pub. Corp. (1959).

[22] W. Shockley, "The Theory of p-n Junctions in Semiconductors and p-n Junction Transistors," *Bell Systems Tech. J.*, **28**, p. 435, (1949).

[23] R. S. Bever and R. L. Sproull, "The Dielectric Constant of Barium Oxide," *Phys. Rev*, **83**, p. 801, (1951).

[24] J. L. Jacobson and E. R. Nixon, "Infrared Dielectric Response and Lattice Vibrations of Calcium and Strontium Oxides," *J. Phys. Chem. Solids*, **29**, p. 967, (1968).

[25] G. A. Saum and E. B. Hensley, "Fundamental Optical Absorption in the IIA-VIB Compounds," *Phys. Rev.*, **113**, p. 1019, (1959).

[26] R. C. Whited and W. C. Walker, "Exciton and Interband Spectra of Crystalline CaO," *Phys. Rev.*, **188**, p. 1380, (1969).

[27] E. A. Coomes, "The Pulsed Properties of Oxide Cathodes," *J. Appl. Phys.*, **17**, p. 647, (1946); B. Ya. Moizhes and S. Sh. Rutshtein, "Breakdown (Sparking) of Oxide Cathodes," *Sov. Phys.-Tech. Phys.*, **16**, p. 1748, (1972).

[28] S. R. Morrison, "Surface Barrier Effects in Adsorption Illustrated by Zinc Oxide," p. 259 in *Advances in Catalysis*, Vol. 7, Academic Press, Inc., New York, (1955).

[29] W. G. Garner, F. S. Stone, and P. F. Tiley, "The Reaction between Carbon Monoxide and Oxygen on Cuprous Oxide at Room Temperature," *Proc. Roy. Soc.*, **A211**, p. 472, (1952); M. Zouaghi, B. Prevot, C. Carabatos and M. Sieskind, "Near Infrared Optical and Photoelectric Properties of Cu_2O," *Phys. Stat. Sol.*, **All**, p. 449, (1972).

[30] T. N. Chin and L. A. Boyer, "D.C. Electroluminescence in Hot-Pressed ZnSe Diodes," *Solid-State Electron*, **16**, p. 143, (1973).

[31] H. H. Glascock, Jr., "Thermionic Emission from CaO in Ba Vapor," *Surface Sci.*, **29**, p. 291, (1972).

[32] L. Apker, E. Taft, and J. Dickey, "On the Photoelectric Emission and Energy Structure of BaO," *Phys. Rev.*, **84**, p. 508, (1951).

[33] K. S. Beynar and B. P. Nikonov, "The Emission and Adsorption Properties of the BaO-Ba, SrO-Ba and CaO-Ba Systems," *Radio Eng. Electron, (USSR)*, **10**, p. 408, (1965), (english translation).

[34] J. B. Taylor and I. Langmuir, "The Evaporation of Atoms, Ions and Electrons from Caesium Films on Tungsten," *Phys. Rev.*, **44**, p. 438, (1933); T. Smith, "Cesium Adsorption on W:Ellipsometry, Auger Spectroscopy, and Surface Potential Difference Studies," *J. Appl. Phys.*, **43**, p. 2964, (1972).

[35] A. Rose, *Concepts in Photoconductivity and Allied Problems*, p. 134, John Wiley and Sons, New York, (1963).

[36] J. S. Blakemore, *Semiconductor Statistics*, p. 175, Pergamon Press, Inc., Elmsford, New York, (1962).

[37] J. W. Gadzuk and E. W. Plummer, "Field Emission Energy Distribution (FEED)," *Rev. Mod. Phys.*, **45**, p. 527, (1973).